PAPER

An old tool to obtain new polymers from renewable resources: [OSSO]-type titanium-catalysed ethylene and myrcene copolymers†

Fatemeh Niknam,[a] Antonio Buonerba, [ID] [abc]
David Hermann Lamparelli*[a] and Carmine Capacchione [ID] *[abc]

The copolymerization of β-myrcene (**M**) with ethylene (**E**) and isoprene (**I**) was successfully promoted by a dichloro{1,4-dithiabutanediyl-2,2′-bis(4,6-di-alkylphenoxy)}titanium complex (**1**) activated by methylaluminoxane (**MAO**). The catalytic system afforded well-defined **PME** copolymers and novel **PMEI** terpolymers with controlled compositions (up to 49% of terpene incorporated in the case of **PME**). Microstructural analysis demonstrated high stereoselectivity of **1**, with 1,4-*trans* insertion predominating for both isoprene (97%) and myrcene (94%). A comprehensive analysis by ^{13}C and 2D NMR techniques confirmed a multi-block architecture for the novel synthesized copolymers. Notably, **PMEI** terpolymers exhibited a strong tendency toward forming alternating ethylene–isoprene (E–I) sequences. The thin film morphology, investigated by tapping mode atomic force microscopy (AFM), for the **PME** and **PMEI** copolymers, evidenced a phase-separated morphology consisting of soft and hard phases, respectively, ascribed to polydienic and polyethylenic domains. The materials displayed glass transition temperatures ranging from −62 to −74 °C, demonstrating their potential as sustainable and high-performance elastomers.

1. Introduction

The quest for more sustainable polymers from bio-based feedstock has emerged as a critical research frontier across polymer chemistry, catalysis, and synthetic chemistry.[1–4] This growing interest is driven by the pressing need to reduce

[a]*Department of Chemistry and Biology "Adolfo Zambelli", University of Salerno, Via Giovanni Paolo II, 132, 84084, Fisciano, SA, Italy. E-mail: ccapacchione@unisa.it; dlamparelli@unisa.it*

[b]*Interuniversity Consortium of Chemical Reactivity and Catalysis (CIRCC), Via Celso Ulpiani, 27, 70126 Bari, Italy*

[c]*Research Centre for Nanomaterials and Nanotechnology (NANO_MATES), Via Giovanni Paolo II, 132, 84084, Fisciano, SA, Italy*

† Electronic supplementary information (ESI) available. See DOI: https://doi.org/10.1039/d5fd00046g

dependence on fossil-derived resources and develop eco-friendly materials with advanced functional properties. Among the various bio-based monomers under investigation, terpenes (especially monoterpenes) have emerged as promising candidates due to their natural abundance and chemically versatile structures.[5–9] These monomers, composed of isoprene units, offer unique opportunities for specific polymerization, crucial for producing materials with well-defined and high-performance properties. A prominent example is myrcene (**M**) (7-methyl-3-methylene-1,6-octadiene; Scheme 1),[10,11] obtained from plant-derived essential oils, primarily through the pyrolysis of β-pinene,[12,13] a significant component of turpentine. Myrcene's conjugated diene structure makes it a versatile building block for polymerization through various mechanisms, including radical, anionic, and coordination polymerization.[14–19]

When copolymerized with styrene (**S**), **M** contributes to synthesizing advanced elastomers, like **S**-butadiene (**B**) and **S**-isoprene (**I**) rubbers, exhibiting characteristics suitable for various applications, such as tyres, automotive components, footwear, adhesives, and gaskets.[6,20–23] Ethylene (**E**) incorporation into such copolymers can enhance thermal and tensile properties, but its copolymerization with conjugated dienes is challenging due to their differing reactivities for a given catalyst.[24,25] Indeed, conjugated dienes may inhibit catalysts meant for simple olefin polymerization, complicating the process.[26,27]

In a pioneering study, Hou and coworkers reported copolymers of **M** with **E** (∼1 bar) and propylene for the first time by using three half-sandwich scandium
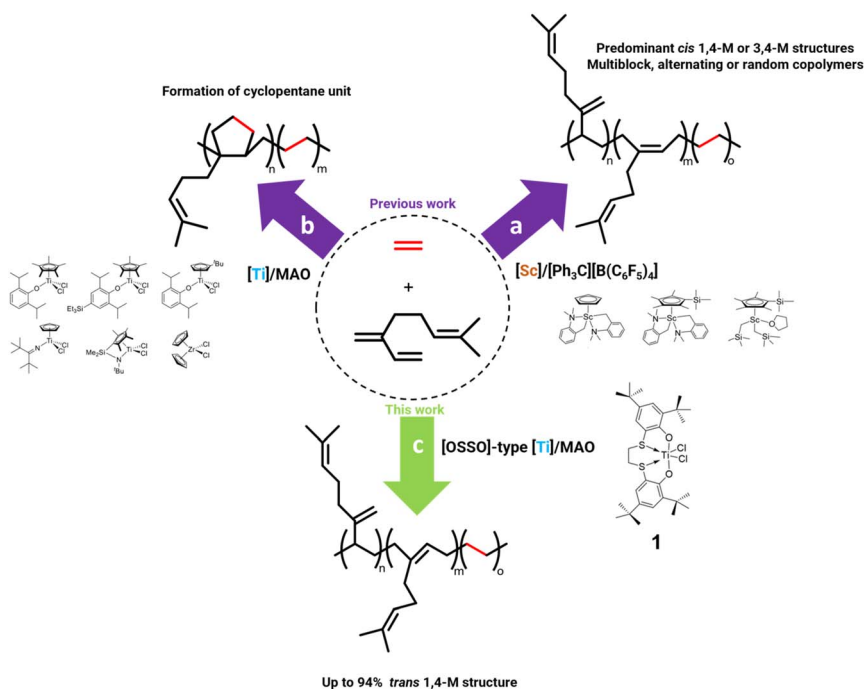
Scheme 1 Myrcene–ethylene copolymerizations: (a) promoted by Sc–based complexes (Guo and Hou);[28] (b) promoted by Ti and Zr half-metallocenes and metallocenes;[31] (c) promoted by an [OSSO]–type bis(phenolate) Ti complex (**1**) (this study).

complexes (see Scheme 1), yielding different block structures depending on the catalyst's ligand size and THF presence.[28] However, the high cost and handling difficulties associated with rare-earth metal catalysts limit their scalability and industrial applicability.

In this context, titanium-based catalysts represent a promising and sustainable alternative. Titanium is the third most abundant metal in Earth's crust that offers advantages in terms of cost, environmental impact, low toxicity and ease of handling in homogeneous catalysis.[29,30] At ~4 bar of **E** pressure, Nomura *et al.* synthesized **E/M** copolymers using half-titanocene catalysts, Cp*TiCl$_2$(O-2,6-^{i}Pr$_2$-4-RC$_6$H$_2$) [R = H or SiEt$_3$], and methylaluminoxane (**MAO**) as cocatalyst (see Scheme 1).[31] The copolymers exhibited promising elastic properties and contained cyclopentane units with a **M** side chain (–CH$_2$CH=CMe$_2$), formed through a 2,1- or 1,4-**M** insertion, which then cyclized after the **E** insertion. However, research on the copolymerization of **M** with **E** is limited, and the role of Ti-based catalysts remains largely unexplored.

This study reports on the copolymerization of **E** with **M** along with the unprecedented *ter*-polymerization with **I**, employing an [OSSO]-type bis(phenolate) titanium complex **1** (see Scheme 1) activated by **MAO**. The C$_2$-bridged [OSSO] titanium complex **1** stands as an exceptionally versatile catalyst. It efficiently polymerizes **E**, α-olefins, and **S**, the latter yielding highly isotactic **PS**.[32–34] Furthermore, complex **1** stereoselectively converts **I**, **B**, and **M** into polydienes enriched in *trans*-1,4 linkages.[21,35] Beyond homopolymerization, it generates diverse copolymers, including **E–S** copolymers, alternating **E–B** and **E–I** elastomers, as well as multiblock copolymers such as **S–B**, **S–M**, and **S–I**.[36] These multiblock copolymers uniquely fuse isotactic **PS** blocks with *trans*-1,4 diene segments. Most recently, the catalyst's scope has expanded to include cyclic vinyl monomers such as 1-vinylcyclohexene (**VCH**), terpene-derived monomers *S*-4-isopropenyl-1-vinyl-1-cyclohexene (**IVCH**)[37] and 3-methylene-cyclopentene,[38] producing highly isotactic or regioregular polymers from these renewable feedstocks.

Under 1 bar of ethylene pressure in toluene at 70 °C, complex **1** enables precise control over the polymerization process. Using this approach, **E–M** copolymers with controllable compositions and precise stereoselectivity were successfully synthesized, achieving particularly high *trans*-1,4 selectivity in the case of **M** units (up to 95%). Detailed characterizations of the materials were performed, focusing on their microstructures, thermal properties, and polymer morphology. The resulting materials exhibit remarkably low glass transition temperatures (from −62 to −74 °C), positioning them as more competitive, sustainable alternatives to full petroleum-based counterparts.

2. Results and discussion

2.1 Copolymerizations of myrcene with ethylene

Copolymerization is a powerful tool to tailor polymer properties by combining different monomers into a single chain. Thermal behaviour, crystallinity, and mechanical performance can be precisely tuned by selecting specific comonomers and controlling their incorporation. This strategy enables the design of advanced materials with customized functionality, surpassing the limitations of homopolymers.[39] The catalyst **1** (Scheme 1), activated by **MAO**, demonstrated its

Table 1 Copolymerization of β-myrcene (**M**) and ethylene (**E**) promoted by catalyst **1**/MAO

Run[a]	**M**/Ti feed[b]	Yield (g)	Activity (kg mol$_{Ti}^{-1}$ h^{-1})	TOF (h^{-1})	$M_w{}^c$ (kDa)	$Đ^c$	$T_g{}^d$	Composition[e]	
								M (mol%)	**M^T**/**M^V** (mol ratio)
1[f]	500	2.01	1.4	38	17.0	1.6	−62.0	100	92/8
2	1000	1.22	12.7	157	14.7	1.5	−67.4	49	89/11
3	500	0.84	8.8	121	11.9	1.6	−69.8	41	90/10
4	350	0.65	6.8	112	8.9	1.7	n.d.[g]	30	92/8
5	250	0.58	6.0	110	8.0	1.8	−71.8	25	92/8
6	180	0.45	4.7	99	6.7	1.7	−72.9	18	93/7
7	70	0.24	2.5	61	4.6	1.6	−74.2	12	93/7

[a] Reaction conditions: catalyst **1** = 10 mg (1.6×10^{-5} mol), P(ethylene)$_0$ = 1 bar, [Al]/[Ti] = 500, toluene (15 mL), 70 °C, 6 h. [b] **M**/Ti initial molar ratio. [c] Determined by GPC. [d] Determined by DSC. [e] Polymer composition determined by ^{1}H NMR (25 °C, CDCl$_3$); for further details see the ESI.† [f] Without ethylene, 24 h. [g] n.d. = not determined.

ability to promote the **M** homopolymerization at 70 °C with remarkable stereo-selective control, yielding 92 mol% of 1,4-*trans* units (**M^T**) and 8 mol% of 3,4-units (**M^V**) in the polymer backbone (run 1, Table 1).[20]

   The high *trans*-1,4 selectivity observed for myrcene aligns with prior reports for 1,3-dyene polymerization, such as 1,3-butadiene and isoprene polymerizations using the same [OSSO]-Ti catalyst system.[21,35,40] This stereoselectivity arises from the catalyst's rigid C$_2$-symmetric geometry, which enforces an allylic mechanism involving *syn*-η^3 chain propagation and *s-trans*-η^2 monomer insertion. Computational studies confirmed that this pathway minimizes steric repulsions, favouring *trans*-1,4 enchainment over *cis* or 1,2 motifs (Scheme 2).[41]
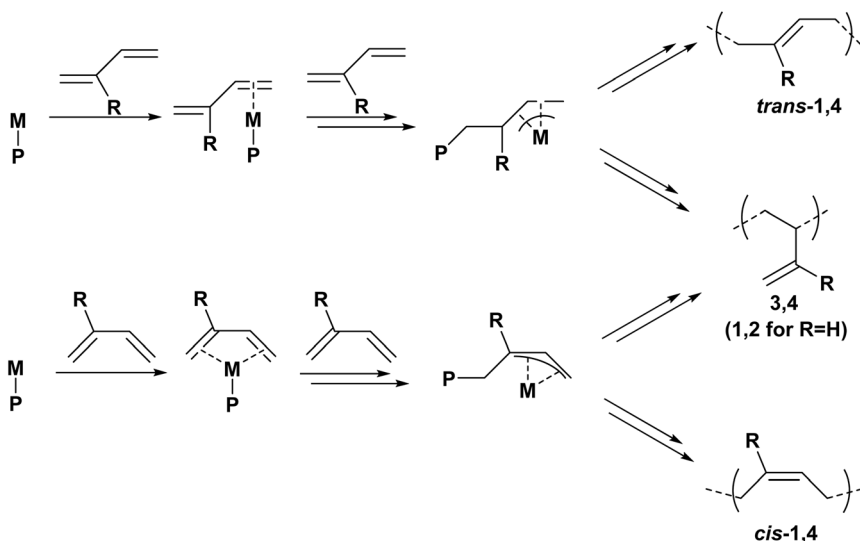
Scheme 2   Regiocontrol in 1,3-diene polymerizations.

The Ti-based complex **1** was also found active in the copolymerization of **M** with **E** under an initial ethylene pressure of 1 bar. The data for the **M**–**E** copolymers (**PME**) promoted by the **1**/**MAO** catalytic system are reported in Table 1. Catalyst performance is reported as conventional activity (expressed in $kg_{polymer}$ mol_{Ti}^{-1} h^{-1}) and turnover frequency (TOF, h^{-1}).

Yields and molecular weights (Table 1) progressively increased with the **M** content in the alimentation feed. Unimodal gel permeation chromatography (GPC) traces, with narrow dispersity values (*Đ*), were found for the copolymers from runs 2–7 of Table 1. The diffusion-ordered NMR spectroscopy (DOSY) analysis (see Fig. S15, ESI†) further confirmed the copolymeric nature of the synthesized materials.

The T_g values of the **PME** copolymers was found in a quite narrow temperature range from −67 to −74 °C (see Table 1 and Fig. 1). A slight decrease in the T_g values was observed for copolymers with a lower **E** content (runs 4–7, Table 1). As the 1,4-*trans* **M** content increases, the copolymer becomes less rigid and more flexible, leading to greater chain mobility. For the sample from run 7 of Table 1, with the highest **E** content (see trace (e) in Fig. 1), in addition to the T_g value of −74.2 °C, a broad melting peak was observed with a melting point temperature (T_m) of 99.9 °C. Reasonably, the higher **E** content leads to the formation of longer **E** segments capable of crystallization.[42] The broad melting endotherm (∼100 °C) indicates imperfect polyethylene-like crystallites of varied sizes, common in random copolymers, where non-uniform segment lengths cause crystals to melt over a wide temperature range.

Polymer compositions were determined by ^1H NMR spectroscopy according to the equations reported in the ESI (see Section 2 of the ESI†). Fig. 2 presents the ^{13}C
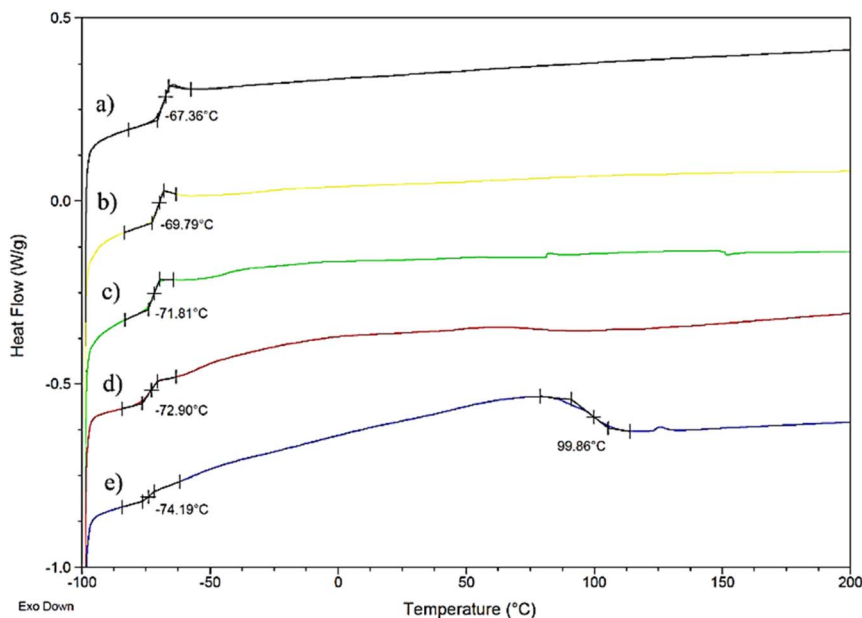

Fig. 1 DSC thermograms of **PME** copolymer from runs 2 (a), 3 (b), 5 (c), 6 (d), and 7 (e) of Table 1.
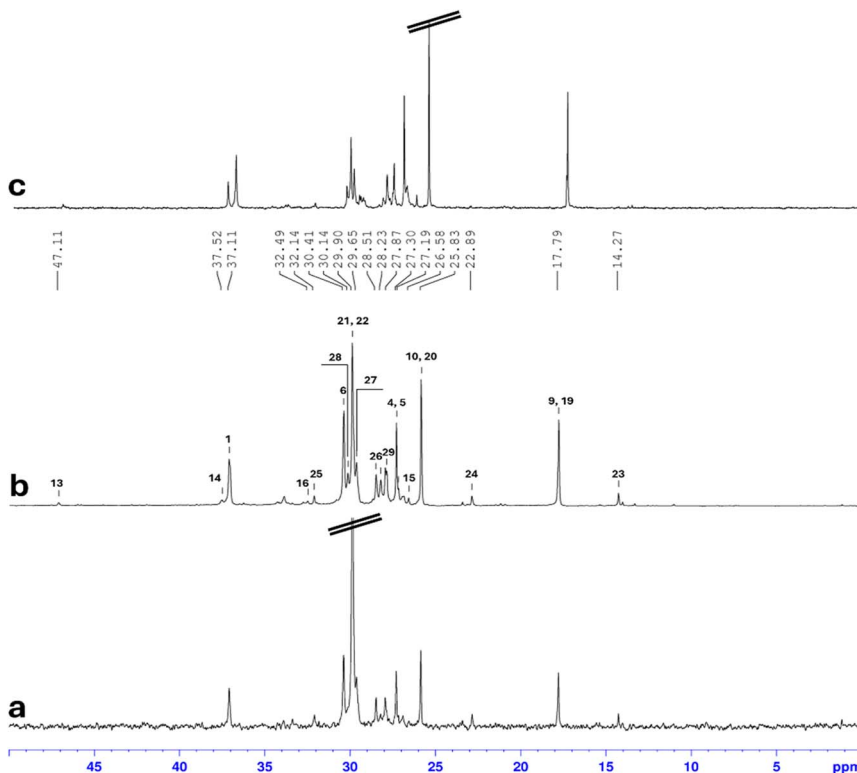
Fig. 2 Aliphatic region of ^{13}C NMR spectra of the **PME** copolymers in Table 1: (a) run 2 (12%$_M$); (b) run 5 (25%$_M$); (c) run 7 (49%$_M$).

NMR spectra of **PME** copolymers with varying **M** content (from 12 to 49 mol%). The comparison of the spectra of the samples from runs 2, 5, and 7 (Table 1) allows clear identification of the main signals, consistent with previous literature reports.[16,20,21,43]

Data analysis shows a multiblock microstructure consisting mainly of 1,4-*trans*-**PM** and **PE** segments. A set of weak signals assignable to the polymer terminal was identified (–**CH$_3$**, 14.27 ppm; –**CH$_2$CH$_3$**, 22.87 ppm; –**CH$_2$CH$_2$CH$_3$**, 32.14 ppm).
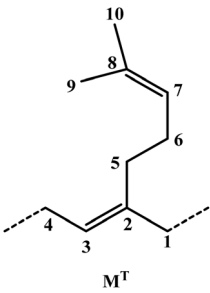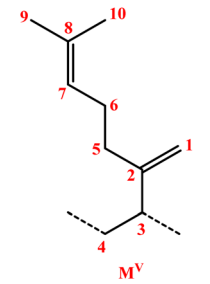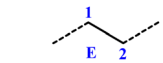
Furthermore, combining 1D and 2D NMR techniques allowed the assignment of several signals corresponding to the junctions between the comonomer blocks. For instance, the signals at 28.23 and 28.51 ppm (line 26, Table 2) obtained *via* heteronuclear single quantum correlation (HSQC) were identified as methylene groups (Fig. S13, ESI†).

The analysis of the heteronuclear multiple bond correlation spectrum (HMBC) revealed correlations between these methylene carbons and protons in the 1.25–1.45 ppm and 1.80–2.20 ppm regions (Fig. S14, ESI†), which are associated with polyethylene sequences and the **M$^T_1$** unit, respectively.

These findings confirm the signals as belonging to either **M$^T_1$E$_1$E** or **EE$_2$M$^T_1$** carbons linked to a 1,4-*trans* **M** unit. Similarly, the **M^{T}M$^T_4$E** junction (line 29, Table 2) could also be identified using HMBC correlation data (Fig. S14, ESI†). The complete assignments for the **PME** copolymers are detailed in Table 2.

Faraday Discussions

Table 2 NMR assignments for **PME** synthesized with **1**/MAO (run 5, Table 1)

Unit[a]	Line	Atom	$^1H^a$ (ppm)	$^{13}C^a$ (ppm)
$\mathbf{M^T}$	1	$\mathbf{M^T_1}$	1.80–2.20	37.11
	2	$\mathbf{M^T_2}$	—	139.18
	3	$\mathbf{M^T_3}$	5.12, 5.15	124.74
	4	$\mathbf{M^T_4}$	1.80–2.20	27.19
	5	$\mathbf{M^T_5}$	1.80–2.20	27.30
	6	$\mathbf{M^T_6}$	1.80–2.20	30.41
	7	$\mathbf{M^T_7}$	5.12, 5.15	125.26
	8	$\mathbf{M^T_8}$	—	131.44
	9	$\mathbf{M^T_9}$	1.62	17.79
	10	$\mathbf{M^T_{10}}$	1.70	25.83
$\mathbf{M^V}$	11	$\mathbf{M^V_1}$	4.74, 4.78	109.17
	12	$\mathbf{M^V_2}$	—	152.17
	13	$\mathbf{M^V_3}$	1.80–2.20	47.11
	14	$\mathbf{M^V_4}$	1.80–2.20	37.52
	15	$\mathbf{M^V_5}$	1.80–2.20	26.58
	16	$\mathbf{M^V_6}$	1.80–2.20	32.49
	17	$\mathbf{M^V_7}$	5.12, 5.15	125.15
	18	$\mathbf{M^V_8}$	—	131.24
	19	$\mathbf{M^V_9}$	1.62	17.79
	20	$\mathbf{M^V_{10}}$	1.70	25.83
$\mathbf{E}$	21	$\mathbf{E_1}$	1.27	29.90
	22	$\mathbf{E_2}$	1.27	29.90
	23	$-\mathbf{CH_3}$ end-group	0.90	14.27
	24	$\mathbf{EE_2CH_3}$ end-group	1.25–1.35	22.88
	25	$\mathbf{EE_1CH_3}$ end-group	1.26–1.32	32.13
	26	$\mathbf{M^T_1E_1E}$ or $\mathbf{EE_2M^T_1}$	1.25–1.45	28.23–28.51
	27	$\mathbf{M^T_4E_2E}$	1.25	29.65
	28	$\mathbf{M^T_1E_2E}$ or $\mathbf{M^T_4E_1E}$	1.18–1.40	30.15
	29	$\mathbf{M^TM^T_4E}$	1.80–2.20	27.87–27.94

^{a} CDCl$_3$, 25 °C, 400 MHz.

The thermogravimetric analysis (TGA) (N$_2$, 10 °C min^{-1}) revealed excellent thermal stability for the synthesized materials, with a single-stage degradation profile (Fig. S34, ESI†). Initial decomposition ($T_{5\%}$) began at 320 °C, with <5% mass loss below 370 °C. Complete degradation occurred at 400–450 °C without residue formation, demonstrating suitability for high-temperature applications.

2.2 Terpolymerizations of myrcene with ethylene and isoprene

Considering the previous results, the catalytic behaviour of **1**/MAO was also evaluated in the terpolymerization of **M** with **E** and isoprene (**I**). Similarly to the above-mentioned **PME** copolymerizations, the reactions were conducted at 70 °C, and different monomer ratios were investigated. The main results are summarized in Table 3. To the best of our knowledge, the terpolymerization of **M**, **E**, and **I**

Table 3 Terpolymerization of β-myrcene (M) with ethylene (E) and isoprene (I)

Run[a]	M feed[b] (mol%)	I feed[b] (mol%)	Activity (kg mol$_{Ti}^{-1}$ h^{-1})	TOF (h^{-1})	Yield (g)	M_w^c (kDa)	$Đ^c$	Polymer composition[d]			
								I/M/E (mol%)	I^T/I^V (mol ratio)	M^T/M^V (mol ratio)	T_g^e (°C)
8	1000	100	11.9	160	1.14	8.3	2.1	5/41/54	95/5	92/8	−72.6
9	500	500	9.2	144	0.88	6.7	2.3	24/24/52	94/6	94/6	−72.7
10	100	1000	8.3	159	0.80	5.5	2.6	50/4/46	97/3	93/7	−74.3

[a] Reaction conditions: catalyst **1** = 10 mg (1.6 × 10^{-5} mol), P(ethylene)$_0$ = 1 bar, [Al]/[Ti] = 500, toluene (15 mL), 70 °C, 6 h. [b] **M**/Ti molar ratio. [c] Determined by GPC. [d] Polymer composition determined by NMR (25 °C, CDCl$_3$); for further details see the ESI.† [e] Determined by DSC.

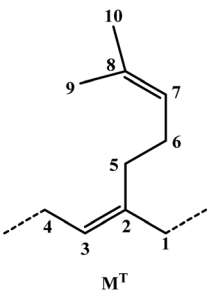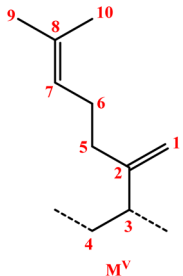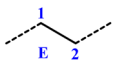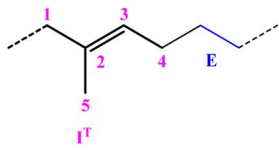**Table 4** NMR assignments for **PMEI** synthesized with **1**/MAO (run 9, Table 3)
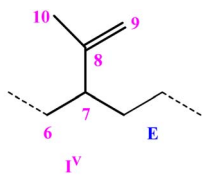
Unit[a]	Line	Atom	$^1H^a$ (ppm)	$^{13}C^a$ (ppm)
	1	M^T_1	1.80–2.20	37.12
	2	M^T_2	—	139.20
	3	M^T_3	5.12, 5.15	124.74
	4	M^T_4	1.80–2.20	27.17
	5	M^T_5	1.80–2.20	27.29
	6	M^T_6	1.80–2.20	30.39
	7	M^T_7	5.12, 5.15	125.25
	8	M^T_8	—	131.28
	9	M^T_9	1.62	17.80
	10	M^T_{10}	1.70	25.85
	11	M^V_1	4.74, 4.78	109.12
	12	M^V_2	—	152.20
	13	M^V_3	2.00	47.07
	14	M^V_4	1.80–2.20	37.51
	15	M^V_5	1.80–2.20	26.57
	16	M^V_6	1.80–2.20	32.47
	17	M^V_7	5.12, 5.15	125.15
	18	M^V_8	—	131.24
	19	M^V_9	1.62	17.80
	20	M^V_{10}	1.70	25.85
	21	E_1	1.27	29.90
	22	E_2	1.27	29.90
	23	I^T_1	1.80–2.20	39.81
	24	I^T_2	—	135.25
	25	I^T_3	5.05–5.25	124.98
	26	I^T_4	1.80–2.20	27.84–28.34
	27	I^T_5	1.60	16.03
	28	I^V_6	1.15–1.45	33.40–33.69
	29	I^V_7	2.00	47.43
	30	I^V_8	—	148.03
	31	I^V_9	4.66, 4.72	111.37

Table 4   (Contd.)

Unit[a]	Line	Atom	^{1}H[a] (ppm)	^{13}C[a] (ppm)
	32	$\mathbf{I^V_{10}}$	1.54–1.72	17.98
	33	$\mathbf{-CH_3}$ end-group	0.90	14.29
	34	$\mathbf{EE_2CH_3}$ end-group	1.25–1.35	22.85
	35	$\mathbf{EE_1CH_3}$ end-group	1.26–1.32	32.13
	36	$\mathbf{M^T_1E_1E}$ or $\mathbf{EE_2M^T_1}$	1.15–1.45	28.21–28.48
	37	$\mathbf{M^T_4E_2E}$	1.28	29.68
	38	$\mathbf{M^T_1E_2E}$ or $\mathbf{M^T_4E_1E}$	1.18–1.40	30.16
	39	$\mathbf{M^TM^T_4E}$	1.80–2.20	27.84–27.96
	40	$\mathbf{M^T_1I^T_1}$ $\mathbf{I^T}$	1.95–2.15	40.27

[a] CDCl$_3$, 25 °C, 400 MHz.

has not been reported before, making our work the first to explore this combination.

The myrcene–ethylene–isoprene terpolymers (**PMEI**) exhibit a monomodal molecular weight distribution with Đ values of 2.1–2.6 and a molecular weight ranging from 5.5 to 8.3 kDa. The narrow dispersity is consistent with a single-site catalytic system, further supporting the copolymeric nature of the material. These findings are verified by DOSY NMR analysis (Fig. S25, ESI†), which confirms the homogeneous incorporation of the comonomers into the polymer backbone without detectable homopolymers. As previously reported, catalyst **1** promotes the polymerization of isoprene (**I**), yielding a polymer with a predominantly *trans*-1,4 microstructure (94%) and a minor fraction of 3,4-units.[40] The microstructure of **PMEI** was characterized using ^{1}H, ^{13}C, DEPT-135, COSY, HMBC, and HSQC NMR analyses (see Fig. S16–S18† for representative spectra). However, due to the structural similarity between **M** and **I** units undergoing analogous insertion modes (*trans*-1,4 and 3,4 additions), significant signal overlap in the ^{1}H NMR spectra complicated direct integration-based compositional analysis. To resolve this ambiguity, polymer compositions were determined using quaternary carbon signals from concatenated units ($\mathbf{M^T_2}$ at 139.20 ppm, $\mathbf{M^V_2}$ at 152.20 ppm, $\mathbf{I^T_2}$ at 135.25 ppm, and $\mathbf{I^V_8}$ at 148.03 ppm, Table 4) and ethylene sequences (see the ESI, Section 2, eqn (E5)–(E7)†). A detailed analysis of the ^{13}C NMR spectra (Fig. 3) provided insight into the distribution of repeating units along the polymer chain, revealing a multiblock structure with short ethylene and myrcene blocks and alternating ethylene–isoprene (**E–I**) sequences, consistent with prior
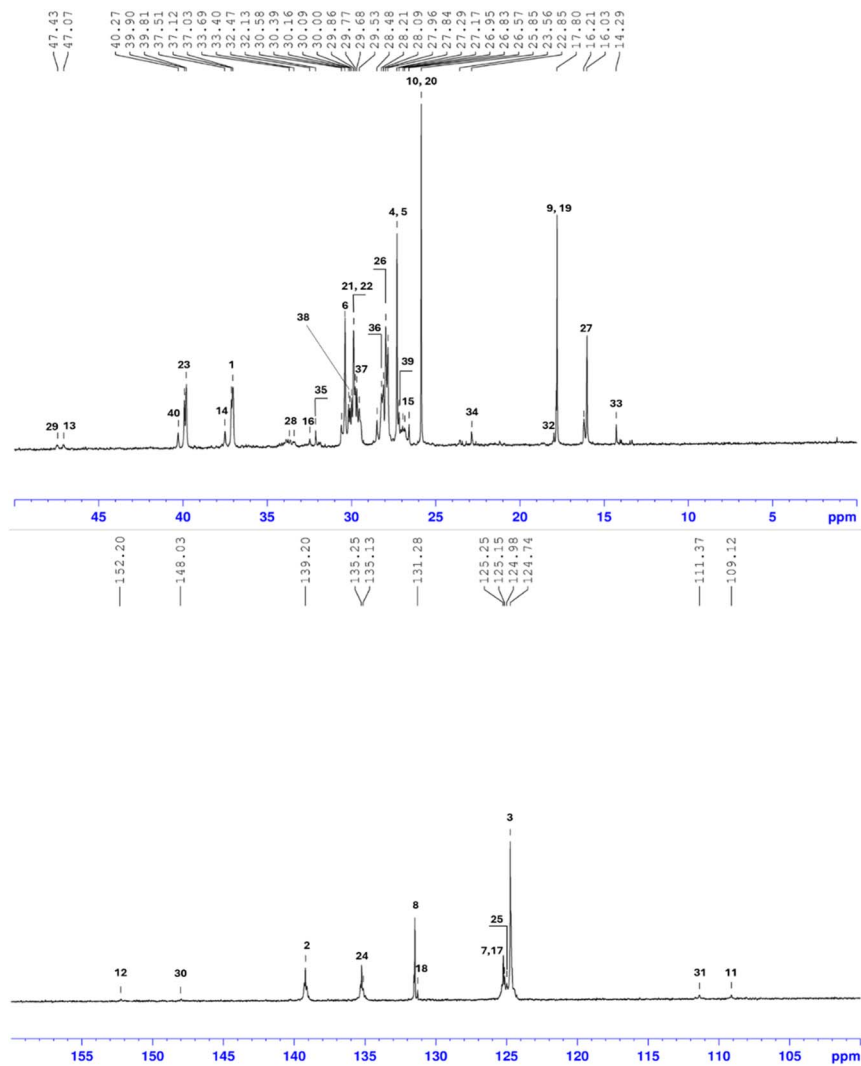
Fig. 3 Aliphatic (on the top) and olefinic (on the bottom) regions of $^{13}C\{^1H\}$NMR spectra of PMEI terpolymers (run 9, Table 3).

observations.[40,43] The complete NMR assignments for these polymers are summarized in Table 4, including key signals corresponding to junction points between comonomer blocks (entries 33–40).

All these terpolymers displayed in the DSC thermal analysis a single T_g between −72.6 and −74.3 °C (Fig. S31–S33, ESI†), with no detectable melting temperature associated with polyethylene blocks. In contrast to high-ethylene PME copolymers, which retain a broad PE melting endotherm, introducing I truncates the E runs, promotes quasi-alternating E–I dyads, and abolishes detectable crystallinity. These results indicate that the amorphous terpolymers exhibit outstanding low-temperature performance. TGA analysis (N$_2$, 10 °C min^{-1}) showed that the PMEI undergoes single-step degradation above 350 °C

$(T_5\%)$, with <5% mass loss at 360 °C, demonstrating high thermal stability (Fig. S35–S37, ESI†).

2.3. Polymer thin film morphology

The surface morphologies of thin films made from the **PM** homopolymer (sample from run 1, Table 1), **PME** (sample from run 5, Table 1), and **PMEI** copolymers (sample from run 9, Table 3) were examined using atomic force microscopy (AFM). Imaging was carried out in non-contact tapping mode to emphasize the phase contrast. Polymer thin films were prepared by depositing polymer solutions in chloroform (0.2 wt%) onto glass slides. The resulting thin films had thickness of ≈500 nm (Fig. S46†). All AFM measurements were performed in air at room temperature. Multiple regions of each sample were analysed to verify the uniformity of the surface morphology across the entire film.

The **PM** sample (run 1, Table 1) displayed a very flat and smooth surface, with no evidence of phase segregation (Fig. 4a).
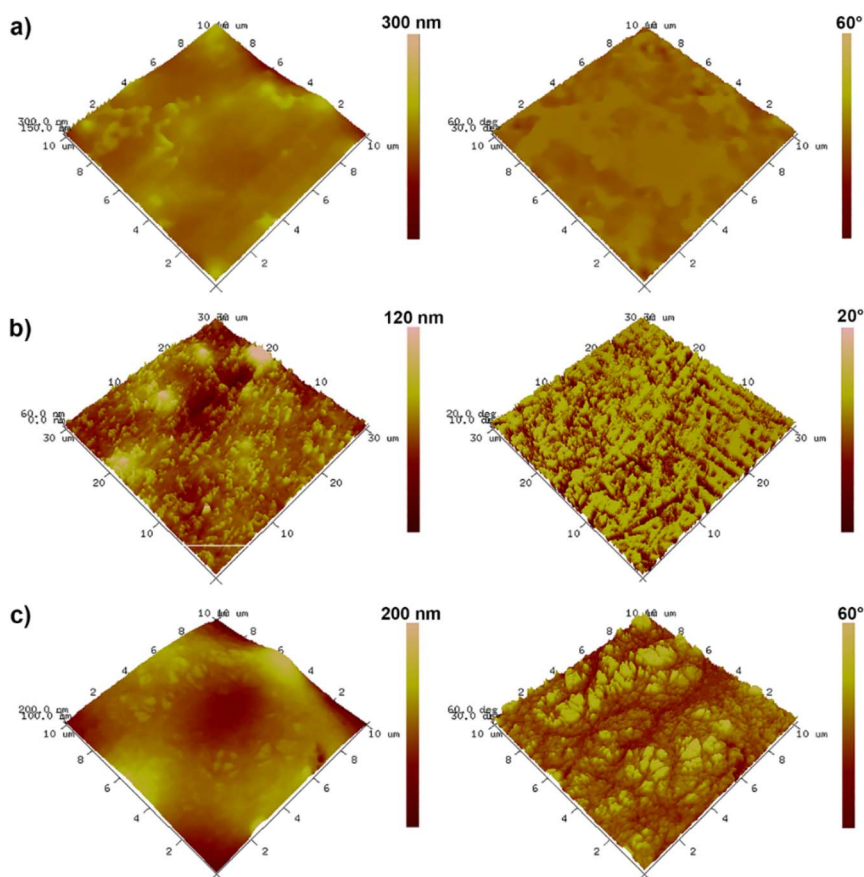

Fig. 4 Height (on the left) and phase contrast (on the right) tapping mode AFM micrographs of (a) **PM** homopolymer (sample from run 1 of Table 1), (b) **PME** copolymer (sample from run 5 of Table 1), and (c) **PMEI** copolymer (sample from run 9, Table 3).

The height images revealed that **PME** (run 5, Table 1) and **PMEI** (run 9, Table 3) exhibit slight surface roughness (Fig. 4b and c on the left). In the corresponding phase contrast images (Fig. 4b and c on the right), the lighter and darker areas correspond to polymer domains with higher and lower stiffness, respectively, indicating rigid and elastic regions. For the **PME** sample (run 5, Table 1), the phase images show a dominant rigid phase incorporating a softer, more elastic phase (see Fig. 4b on the right). In contrast, the **PMEI** sample (run 9, Table 3) displays a primarily elastic matrix containing domains of a stiffer phase (see Fig. 4c on the right).

The polydiene regions are the most elastic, while the polyethylene regions exhibit greater rigidity. The rigidity contrast is not particularly pronounced, implying that the elastic moduli of the different phases are relatively close in value.

Across all samples, no evidence of raw phase separation was observed, suggesting the formation of copolymeric materials rather than homopolymer blends, further confirming the GPC and DOSY NMR data.

3 Experimental section

3.1 General procedures and materials

Air- and moisture-sensitive compounds were handled under an inert nitrogen atmosphere using standard Schlenk line techniques or within an MBraun glovebox. Before use, all glassware was dried in an oven at 130 °C and kept under a nitrogen atmosphere. Commercially available toluene (Sigma-Aldrich) was dried over calcium chloride, refluxed under nitrogen for 48 hours with sodium, and distilled before use. Methylaluminoxane (**MAO**; 10 wt% solution in toluene, Sigma-Aldrich) was used without further purification. β-Myrcene (≥95%) and isoprene were purchased from Sigma-Aldrich and purified by stirring overnight with calcium hydride, followed by distillation under reduced pressure. Ethylene gas for polymerization grade (99.9%) was purchased from Linde Co. and used as received. The dichloro{1,4-dithiabutanediyl-2,2′-bis(4,6-dialkylphenoxy)}titanium complex **1** was prepared according to a previously reported procedure.[44]

3.2 Instrumentation and methods

NMR analysis of polymers was conducted in deuterated solvents at room temperature using Bruker Avance spectrometers operating at 300, 400, or 600 MHz. Using 5 mm (o.d.) NMR tubes, copolymer samples (20 mg) were dissolved in $CDCl_3$ (0.7 mL) and analysed at room temperature. Chemical shifts are expressed in parts per million (ppm, δ) and referenced to the residual solvent signals: $\delta = 7.26$ ppm in ^{1}H NMR and $\delta = 77.16$ ppm in ^{13}C NMR experiments in $CDCl_3$. Spectral acquisition utilized Bruker-TopSpin v2.1 software, while data processing was carried out with TopSpin v2.1 or MestReNova v6.0.2. ^{1}H NMR spectra were acquired using a zg pulse program with a 6.0 μs pre-scan delay, 1 s relaxation delay, and 12.0 ppm spectral width (64 scans). ^{13}C NMR spectra were recorded with a zgpg30 pulse program, using a 6.0 μs pre-scan delay, 2 s relaxation delay, and 220.0 ppm spectral width (32 000 scans). All spectra were processed with an exponential filter (lb = 2 Hz) before Fourier transformation. Baseline correction was applied, and peak integrations were averaged over at least three

measurements. DOSY NMR experiments were performed at 298 K on a Bruker Avance 600 spectrometer using a stimulated echo sequence with bipolar gradients and LED. Gradient strength was linearly ramped from 5% to 95% over 25 min, with optimized parameters: $\Delta = 2500$ ms (diffusion time), $\delta = 1000$ ms (gradient pulse), and eddy current delay = 5 ms. Data processing in Topspin 3.2 included Fourier transformation, baseline correction, and Gaussian fitting to extract diffusion coefficients.

Molecular weights (M_w) and dispersity indices ($Đ$) were determined *via* a 150 C Waters GPC equipped with a RI detector, a JASCO 875-UV (254 nm) detector and a set of four columns from PSS (pore size of 10^6, 10^5, 10^4, and 10^3 Å, particle size of 5 µm). THF was used as mobile phase at a flow rate of 1.0 mL min^{-1}. Commercial polystyrene standards were employed as calibration references, and data analysis was performed using Waters Breeze v3.30 software.

Differential scanning calorimetry (DSC) measurements were performed on a DSC Q20 in aluminium pans under a nitrogen atmosphere, with a heating rate of 10 °C min^{-1}, spanning a temperature range of −80 to +150 °C. Results from the second heating cycle were processed using TA Universal Analysis v2.3 software.

Thermal gravimetric analysis (TGA) was conducted using a TA Instrument Q500 thermogravimetric analyser. The tests were performed in the temperature range of 25–600 °C with a heating rate of 10 °C min^{-1} under a nitrogen flow.

Atomic force microscopy (AFM) images of polymer thin films were acquired in air at room temperature using a Dimension 3100 system paired with a Nano-Scope V controller (Bruker), operating in tapping mode. The films were prepared by depositing chloroform polymer solutions (0.2 wt%) onto glass slides at room temperature. Commercially available probe tips were used, featuring nominal spring constants between 20 and 100 N m^{-1}, resonance frequencies ranging from 200 to 400 kHz, and tip radii of 5–10 nm. Image analysis was performed using Bruker's NanoScope Analysis software (version 190R1sr2, Ettlingen, Germany).

3.3 General M–E copolymerization procedure (referred to run 2, Table 1)

In a 100 mL round-bottom flask equipped with a magnetic stirrer, β-myrcene (2.2 g, 0.016 mol), **MAO** (5.10 mL, 0.0082 mol), and toluene (∼10 mL) were sequentially introduced under an inert atmosphere. The reactor was purged and saturated with ethylene at 1 bar pressure. The reaction mixture was stirred for several minutes and gradually warmed to 70 °C before adding the complex **1** (10 mg, 1.0×10^{-5} mol). After 6 h, the polymerization was quenched by the addition of methanol. The resulting mixture was then poured into an acidified ethanol solution containing butylated hydroxytoluene (**BHT**) as a stabilizer. The precipitated polymer was isolated by filtration, washed thoroughly, and dried under vacuum at room temperature until a constant weight was achieved (yield = 1.22 g).

3.4 General M–E–I terpolymerization procedure (referred to run 9, Table 3)

In a 100 mL round-bottom flask equipped with a magnetic stirrer, toluene, β-myrcene (1.5 g, 0.011 mol), isoprene (1.1 mL, 0.011 mol), **MAO** (5.10 mL, 0.0082 mol), and toluene (∼10 mL) were sequentially introduced under an inert atmosphere. The reactor was purged and saturated with ethylene at 1 bar pressure. The reaction mixture was stirred for several minutes and gradually warmed to 70 °C

before adding the complex **1** (1.0×10^{-5} mol). After 6 h, the polymerization was quenched by the addition of methanol. The resulting mixture was then poured into an acidified ethanol solution containing **BHT** as a stabilizer. The precipitated polymer was isolated by filtration, washed thoroughly, and dried under vacuum at room temperature until a constant weight was achieved (yield = 0.88 g).

4 Conclusions

In this study, the copolymerization of β-myrcene (**M**) with ethylene (**E**) and isoprene (**I**) using an [OSSO]-type titanium complex **1** activated by **MAO** is reported. The catalytic system exhibited remarkable stereoselectivity, yielding **PME** copolymers and **PMEI** terpolymers with a predominantly *trans*-1,4 microstructure (up to 94% for **M** and 97% for **I**).

Comprehensive NMR analyses (^{1}H, ^{13}C, DEPT-135, COSY, HMBC, HSQC) confirmed a well-defined multiblock architecture with homogeneous comonomer incorporation and no detectable homopolymers. **PME** copolymers contained up to 49 mol% of **M**, while **PMEI** terpolymers displayed a clearly alternating ethylene–isoprene sequence.

From a thermal perspective, **PME** copolymers exhibited tuneable T_g values ranging from −62 to −74 °C, with crystallinity observed in samples with high ethylene content ($T_m \approx$ 99 °C). In contrast, **PMEI** terpolymers showed fully amorphous behaviour, with T_g values between −72.6 and −74.3 °C, making them particularly suitable for application as low-temperature elastomers. Thermogravimetric analysis revealed excellent thermal stability, with degradation onset temperatures above 320 °C.

TOF data confirm the high productivity of the **1**/**MAO** catalytic system across all runs, with peak TOF ($\sim 1.6 \times 10^2$ h^{-1}) in the most **E**-rich samples.

The thin film morphology, investigated by tapping mode atomic force microscopy, for the **PME** and **PMEI** copolymers evidenced a phase-separated morphology consisting of elastic and rigid phases, respectively ascribed to polydienic and polyethylenic domains.

Overall, these results highlight the potential of titanium-based catalysts in the synthesis of sustainable and biobased polymers, effectively combining bioderived terpenes with ethylene and isoprene to generate materials with tailored structures and properties for advanced industrial applications.

Data availability

The data supporting this article have been included as part of the ESI.†

Author contributions

F. N.: methodology, investigation, data curation; A. B.: validation, formal analysis, data curation, writing – original draft, writing – review & editing, visualization; D. H. L: conceptualization, methodology, validation, formal analysis, investigation, data curation, writing – review & editing, visualization, supervision; C. C.: conceptualization, validation, formal analysis, investigation, data curation, writing – original draft, writing – review & editing, visualization, supervision, funding acquisition.

Conflicts of interest

The authors declare no competing interests.

References

1 S. A. Miller, *ACS Macro Lett.*, 2013, **2**, 550–554.

2 T. P. Haider, C. Völker, J. Kramm, K. Landfester and F. R. Wurm, *Angew. Chem., Int. Ed.*, 2019, **58**, 50–62.

3 Y. Zhu, C. Romain and C. K. Williams, *Nature*, 2016, **540**, 354–362.

4 M. A. Hillmyer, *Science*, 2017, **358**, 868–870.

5 P. A. Wilbon, F. Chu and C. Tang, *Macromol. Rapid Commun.*, 2013, **34**, 8–37.

6 P. Sahu, A. K. Bhowmick and G. Kali, *Processes*, 2020, **8**, 553.

7 J. Zhao and H. Schlaad, in *Bio-synthetic Polymer Conjugates*, ed. H. Schlaad, Springer Berlin Heidelberg, Berlin, Heidelberg, 2011, vol. 253, pp. 151–190.

8 C. Napolitano, V. Paradiso, M. Naddeo, D. H. Lamparelli, F. Grisi, O. Ruiz De Ballesteros, G. Femina, C. Capacchione and F. Auriemma, *Macromolecules*, 2024, **57**, 7409–7417.

9 F. Della Monica and A. W. Kleij, *Polym. Chem.*, 2020, **11**, 5109–5127.

10 A. Behr and L. Johnen, *ChemSusChem*, 2009, **2**, 1072–1095.

11 P. Sarkar and A. K. Bhowmick, *RSC Adv.*, 2014, **4**, 61343–61354.

12 M. B. Kolicheski, L. C. Cocco, D. A. Mitchell and M. Kaminski, *J. Anal. Appl. Pyrolysis*, 2007, **80**, 92–100.

13 M. Winnacker, *Angew. Chem., Int. Ed.*, 2018, **57**, 14362–14371.

14 S. Choi and H. Ritter, *e-Polym.*, 2007, 7, 045, DOI: **10.1515/epoly.2007.7.1.527**.

15 D. H. Lamparelli, M. M. Kleybolte, M. Winnacker and C. Capacchione, *Polymers*, 2021, **13**, 838.

16 S. Loughmari, A. Hafid, A. Bouazza, A. El Bouadili, P. Zinck and M. Visseaux, *J. Polym. Sci., Part A: Polym. Chem.*, 2012, **50**, 2898–2905.

17 D. H. Lamparelli, M. Winnacker and C. Capacchione, *ChemPlusChem*, 2022, **87**, e202100366.

18 N. Bauer, J. Brunke and G. Kali, *ACS Sustainable Chem. Eng.*, 2017, **5**, 10084–10092.

19 D. H. Lamparelli, V. Paradiso and C. Capacchione, *Rubber Chem. Technol.*, 2020, **93**, 605–614.

20 M. Naddeo, A. Buonerba, E. Luciano, A. Grassi, A. Proto and C. Capacchione, *Polymer*, 2017, **131**, 151–159.

21 D. H. Lamparelli, V. Paradiso, F. D. Monica, A. Proto, S. Guerra, L. Giannini and C. Capacchione, *Macromolecules*, 2020, **53**, 1665–1673.

22 J. Zhang, J. Lu, K. Su, D. Wang and B. Han, *J. Appl. Polym. Sci.*, 2019, **136**, 48159.

23 P. Sarkar and A. K. Bhowmick, *J. Appl. Polym. Sci.*, 2018, **135**, 45701.

24 J. Thuilliez, V. Monteil, R. Spitz and C. Boisson, *Angew. Chem.*, 2005, **117**, 2649–2652.

25 B. Sun and B. Liu, *Macromolecules*, 2024, **57**, 6914–6926.

26 L. Porri and A. Giarrusso, in *Comprehensive Polymer Science and Supplements*, Elsevier, 1989, pp. 53–108.

27 G. Ricci, G. Pampaloni, A. Sommazzi and F. Masi, *Macromolecules*, 2021, **54**, 5879–5914.

28 X. Ren, F. Guo, H. Fu, Y. Song, Y. Li and Z. Hou, *Polym. Chem.*, 2018, **9**, 1223–1233.

29 V. C. Gibson and S. K. Spitzmesser, *Chem. Rev.*, 2003, **103**, 283–316.

30 V. Paradiso, V. Capaccio, D. H. Lamparelli and C. Capacchione, *Catalysts*, 2020, **10**, 825.

31 S. Kitphaitun, S. Chaimongkolkunasin, J. Manit, R. Makino, J. Kadota, H. Hirano and K. Nomura, *Macromolecules*, 2021, **54**, 10049–10058.

32 C. Capacchione, A. Proto and J. Okuda, *J. Polym. Sci., Part A: Polym. Chem.*, 2004, **42**, 2815–2822.

33 C. Capacchione, F. De Carlo, C. Zannoni, J. Okuda and A. Proto, *Macromolecules*, 2004, **37**, 8918–8922.

34 C. Capacchione, A. Proto, H. Ebeling, R. Mülhaupt and J. Okuda, *J. Polym. Sci., Part A: Polym. Chem.*, 2006, **44**, 1908–1913.

35 S. Milione, C. Cuomo, C. Capacchione, C. Zannoni, A. Grassi and A. Proto, *Macromolecules*, 2007, **40**, 5638–5643.

36 V. Paradiso, V. Capaccio, D. H. Lamparelli and C. Capacchione, *Coord. Chem. Rev.*, 2021, **429**, 213644.

37 I. Grimaldi, A. D'Amato, M. C. Gambardella, A. Buonerba, R. Marzocchi, F. Auriemma and C. Capacchione, *Macromol. Rapid Commun.*, 2025, **46**, 2400834.

38 C. Napolitano, V. Paradiso, M. Naddeo, D. H. Lamparelli, F. Grisi, O. Ruiz De Ballesteros, G. Femina, C. Capacchione and F. Auriemma, *Macromolecules*, 2024, **57**, 7409–7417.

39 G. G. Odian, *Principles of Polymerization*, Wiley, Hoboken, N.J, 4th edn, 2004.

40 C. Capacchione, D. Saviello, A. Avagliano and A. Proto, *J. Polym. Sci., Part A: Polym. Chem.*, 2010, **48**, 4200–4206.

41 C. Costabile, C. Capacchione, D. Saviello and A. Proto, *Macromolecules*, 2012, **45**, 6363–6370.

42 G. Guerra, O. R. De Ballesteros, V. Venditto, M. Galimberti, F. Sartori and R. Pucciariello, *J. Polym. Sci., Part B: Polym. Phys.*, 1999, **37**, 1095–1103.

43 S. Loughmari, M. Visseaux, A. Bouazza, A. Hafid and A. El Bouadili, *Arkivoc*, 2009, (xii), 45–59.

44 C. Capacchione, A. Proto, H. Ebeling, R. Mülhaupt, K. Möller, T. P. Spaniol and J. Okuda, *J. Am. Chem. Soc.*, 2003, **125**, 4964–4965.